Research Article Vol. 9, No. 7 / July 2022 / Optica 755

Spatiotemporal sampling of near-petahertz vortex fields

Johannes Blöchl,[1,2] Johannes Schötz,[1,2] Ancyline Maliakkal,[1,2] Natālija Šreibere,[1,2] Zilong Wang,[1,2] Philipp Rosenberger,[1,2] Peter Hommelhoff,[3] Andre Staudte,[4] Paul B. Corkum,[4] Boris Bergues,[1,2] and Matthias F. Kling[1,2,5,6,*]

[1]Department of Physics, Ludwig-Maximilians-Universität Munich, D-85748, Garching, Germany
[2]Max Planck Institute of Quantum Optics, D-85748, Garching, Germany
[3]Laser Physics, Department of Physics, Friedrich-Alexander-Universität Erlangen-Nürnberg, D-91058, Erlangen, Germany
[4]Joint Attosecond Science Laboratory, National Research Council of Canada and University of Ottawa, Ottawa, Ontario K1A0R6, Canada
[5]SLAC National Accelerator Laboratory, Menlo Park, California 94025, USA
[6]Applied Physics Department, Stanford University, Stanford, California 94305, USA
*Corresponding author: kling@stanford.edu

Received 28 March 2022; revised 27 May 2022; accepted 30 May 2022; published 5 July 2022

Measuring the field of visible light with high spatial resolution has been challenging, as many established methods only detect a focus-averaged signal. Here, we introduce a near-field method for optical field sampling that overcomes that limitation by employing the localization of the enhanced near-field of a nanometric needle tip. A probe field perturbs the photoemission from the tip, which is induced by a pump pulse, generating a field-dependent current modulation that can easily be captured with our electronic detection scheme. The approach provides reliable characterization of near-petahertz fields. We show that not only the spiral wavefront of visible femtosecond light pulses carrying orbital angular momentum (OAM) can be resolved but also the field evolution with time in the focal plane. Additionally, our method is polarization sensitive, which makes it applicable to vectorial field reconstruction.

https://doi.org/10.1364/OPTICA.459612

1. INTRODUCTION

The precise knowledge of the electro-magnetic field oscillations of light is not only the backbone of ultrafast science [1,2] but the indispensable prerequisite for many applications such as time-domain terahertz spectroscopy [3–5] and field-resolved mid-infrared spectroscopy [6,7]. Common techniques for field sampling reaching from the near-infrared to the visible spectral region include attosecond streaking [8–14], electro-optic sampling [15], femtosecond streaking [16], nonlinear photoconductive sampling [17], or tunneling ionization with a perturbation for the time-domain observation of an electric field (Tiptoe) [18–25]. The latter is especially appealing due to its simplicity.

While the sampling of electric field waveforms in the time domain is well established, its simultaneous spatial characterization has remained challenging, whereas for terahertz radiation, where the wavelength is much longer than for visible light, sub-focal size resolution can be achieved, for instance, by using cameras [26] or small sensors [27], and spatially resolved field measurements in the focus of a visible light beam are challenging as the typical focal size is of the order of a few micrometers. Here, a sub-micrometer probe is necessary. First demonstrations of the application of the Tiptoe-principle to solids [24,25] and nanostructures [23] have shown the path toward infrared field sampling with small spatial probes. However, the work presented in [23] recorded an averaged signal from up to 15 nanostructures separated by up to 600 nm each, whereas the method for sampling spatiotemporally coupled laser pulses introduced in [25] was limited to long wavelengths in the infrared region and to a precision of the pixel size of their sensor, 5.2 μm.

The importance of spatial resolution in field sampling becomes even more apparent when the field of an optical vortex beam is being sampled. Because of its helical phase, the field has a π phase shift at opposite sides of the orbital angular momentum (OAM) mode [28,29]. Thus, for measurement techniques that are only sensitive to the focal averaged field, a complete cancellation of the signal can be expected. Consequently, the field-resolved measurement of vortex beams requires sub-focal spatial sampling. Several articles report the measurement of the corresponding OAM carried by the light [29–31], but not of the field itself. Sampling the field locally could in principle be achieved in attosecond streaking experiments, where the focal spot size of an extreme ultraviolet beam, used for the generation of a temporal gate, is much smaller than that of the (near-petahertz) field to be sampled. Such experiments have been investigated theoretically [32,33]. However, due to the complexity of these measurements, it is not surprising that the use of attosecond streaking for the spatial reconstruction of near-petahertz vortex fields has not been reported yet. A way to avoid sub-focal probing is to image the field induced electron

emission, which is limited by the resolution of the electron optics only [34,35]. Nevertheless, this approach requires ultra-high vacuum and complicated electron imaging spectrometers, and is not applicable to the sampling of fields in free-space.

To date, approaches using near-field methods to achieve spatial resolution could either not resolve the electric field of light itself [36–39] or were limited to much lower frequency ranges in the terahertz regime [4,5]. So far, the application of Tiptoe to small spatial probes has been limited to a precision of several micrometers [23,25]. Here, we overcome these limitations by employing a single nanometric needle tip as a localized probe for the near-field sampling of femtosecond light fields. The approach, termed nanoTiptoe and illustrated in Fig. 1(a), inherits the method for sampling the electric field from Tiptoe [18] and achieves high spatial resolution from field localization at the nanometric needle tip.

In nanoTiptoe, a few-cycle pump pulse drives electron emission in the tunneling regime that depends nonlinearly on the electric field. Due to this nonlinearity and a short pump pulse, the photoemission is limited to the strongest half-cycle of the laser pulse, and suppressed otherwise. We note that only electric field vectors pointing into the surface cause photoemission from the nanometric needle tip [41]. Similar to Tiptoe, the emission burst during the strongest half-cycle opens a sub-cycle temporal gate that is perturbed linearly with the signal pulse [18], enabling characterization of its field. We measured the resulting photoemission current from the needle tip after transimpedance amplification employing lock-in detection. Importantly, the fields driving photoemission were the locally enhanced near-fields, which were strongest near the apex of the tip, cf. Fig. 1(b). The current measurement approach makes complex ultra-high-vacuum-based time-of-flight spectroscopy with nanometric needle tips [37,42] obsolete. Additionally, the localization at the nanometric needle tip exceeds conventional (Tiptoe) methods regarding the precision in space.

2. EXPERIMENTAL DETAILS

The output of a commercial 10 kHz Ti:Sa chirped pulse amplifier is broadened in a hollow-core fiber to an octave spanning spectrum ranging from 500 nm to 1000 nm, with a central wavelength of 750 nm. The pulses are then compressed to a duration of around 4.2 fs using chirped mirrors (UFI PC70). The laser beam was actively stabilized in angle and position. The pulses were split into a strong pump pulse and a weak signal pulse in a Mach–Zehnder interferometer [not shown in Fig. 1(a)], where the signal pulse is chopped at half the repetition rate. To facilitate the precise control of the delay between signal and pump pulses, the pump arm is provided with a retro-reflector mounted on a closed-loop piezo-stage (MCL OPM100) with 100 µm travel range. The beams were focused with variable temporal delay onto a nanometric tungsten needle tip inside a vacuum chamber (2×10^{-3} mbar) using an off-axis parabolic mirror (OAP, $f = 101.6$ mm). For the shadow image in Fig. 1(c), we used $f = 25.4$ mm to get a sharper contour.

The needle was directly soldered to a BNC pin, which was mounted onto a 3D closed-loop piezo stick-slip stage. The photocurrent is amplified by 10^9 V/A using a low-noise high-gain transimpedance amplifier (FEMTO DLPCA-200) and detected using a lock-in amplifier (Zürich Instruments HF2LI). The upper cutoff frequency ($f_{-3\,\mathrm{dB}}$) of the transimpedance amplifier is 1.1 kHz, which is below the repetition rate of our laser of 10 kHz and 5 kHz for pump and signal beam, respectively. The expected damping of the signal can be estimated from the measured amplifier response curve provided by the manufacturer to −20 dBV and −14 dBV for 10 and 5 kHz, respectively. These values correspond to a damping factor of the voltage signal of 10 and 5, in that order. Whenever we estimated a number of emitted electrons, we took

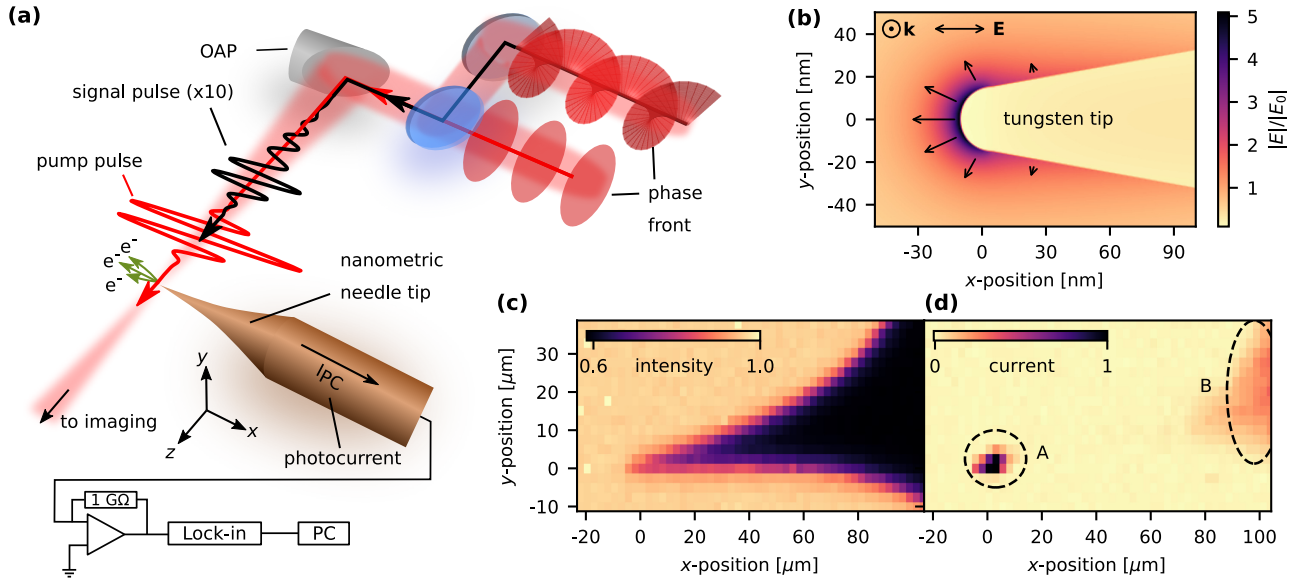

Fig. 1. nanoTiptoe approach for spatiotemporal field sampling: (a) Experimental setup: The pump pulse (red line) and signal pulse (black line) were focused onto a tungsten tip with an off-axis parabola (OAP). The photocurrent generated by the emitted electrons was trans-impedance amplified and lock-in detected. (b) Finite-difference time-domain simulations of the field around an exemplary tungsten tip with 10.5° half-opening angle and a radius of $r =$ 15 nm have shown that the field is enhanced by a factor of around 5, in agreement with literature values [40]. The arrows indicate the near-field polarization. (c). Shadowgraphy image obtained by scanning the tip across the x, y plane while detecting the transmitted intensity. The opening angle in the experiment was determined to be $(21 \pm 2)°$. (d) Detected ionization current as a function of position. The signal in region A corresponds to the ionization at the apex, whereas the signal in region B is due to a small contribution from ionization near the rear-end of the needle shank, which can be spatially discriminated.

these factors into account. For the lock-in detection, we used a demodulation bandwidth of 1.459 Hz ($f_{-3\mathrm{dB}}$). From a noise reference measurement with blocked laser beams, we calculated the normalized noise density to 4.8 $\mu V/\sqrt{Hz}$ and 4.2 $\mu V/\sqrt{Hz}$ for the 5 and 10 kHz components, respectively. This is close to the specified value of 4.3 $fA/\sqrt{Hz}$ noise current at our amplification of 10^9 V/A. In order to be detectable, the minimum current modulation, thus, has to be larger than the noise current times the damping, that is, $e \cdot n_e/s > 4.8\,\mathrm{fA} \times 5$. Here, e is the elementary charge, and n_e is the number of electrons. This corresponds to a current modulation of at least 30 electrons per shot, assuming a 1 Hz demodulation bandwidth for illustration purposes. In the high-gain mode of the amplifier, the amplification bandwidth would be even larger, such that damping becomes negligible, and a modulation of only six electrons per shot would become detectable in theory. We found best signal-to-noise performance, however, in the low-noise mode, where the cutoff frequency was below the repetition rate, as discussed earlier. The lock-in detection separates the contributions from pump pulse and signal pulse as they have different repetition rates. We were, therefore, able to directly measure a modulation current without the current caused by the pump beam.

For a reference measurement using conventional Tiptoe, a pair of copper electrodes with a distance of (120 ± 15) μm was employed to detect the total ionization yield in gas (i.e., air at 50 mbar). A bias voltage of 10 V between the electrodes was applied directly by the transimpedance amplifier. The sampling speed was around 10–14 data points per second, corresponding to a time interval longer than the time-constant of the lock-in amplifier of 47 ms. In addition, the data acquisition was paused for 100 ms after each step in space, in order to wait for the decay of currents induced by the movement of the tip.

3. RESULTS AND DISCUSSION

Before performing the actual field measurements, a large raster scan of the nanometric needle tip in the x, y plane in the laser focus was performed to confirm that the current is generated at the apex of the tip with a laser beam polarized along the tip axis [Fig. 1(d)]. Simultaneously, we recorded the transmitted light in an imaging geometry resulting in the shadow image of the tip shown in Fig. 1(c). The comparison of Figs. 1(c) and 1(d) demonstrates that photoemission occurred predominantly at the apex of the needle tip (region A), whereas currents from sharp features at the needle shank (region B) were prevented by suitable positioning of the tip. As there is no emission between region A and B, we conclude that there is no emission from the side of the nanometric needle tip. Emission away from the tip apex occurs in regions characterized by a large surface roughness. Therefore, the distance between A and B corresponds to the upper limit for the size of the scanning region. Based on a broad parameter study [40] and the experimentally determined enhancement of around $5.1^{+1.2}_{-0.9}$ (see Supplement 1), as well as the opening angle ($(21 \pm 2)°$), we estimated an apex radius of the tip of $r = 14^{+11}_{-7}$ nm.

The nanoTiptoe measurement obtained for linearly polarized sample and pump pulses (polarized along the needle direction) with the needle tip placed in the center of the focus is presented in Fig. 2(a). The obtained waveform is compared to a reference obtained via conventional Tiptoe, showing a remarkable agreement.

It is important to remark that, similar to other Tiptoe-type methods, nanoTiptoe offers a waveform measurement that only detects the carrier-envelope-phase (CEP) difference between the pump and signal pulse. This phase effect has been extensively studied in [19,23–25]. Thus, the waveform shown in Fig. 2(a) only represents the actual electric field if the CEP of the pump pulse is chosen such that only a single ionization burst occurs at $t = 0$ (see Supplement 1, Sections 3 and 4 for more details). As both pulses originated from the same source, an overall CEP drift did not affect the measurement.

For very broadband pulses, the spectral amplitude of the nanoTiptoe response is expected to depend on the CEP of the pump pulse ([23–25] and Supplement 1, Section 3). However, the increasing nonlinearity for smaller field strengths (see Supplement 1, Fig. S7) in our experiments suppresses ionization of lower-intense half-cycles even more, such that the spectral response becomes very broadband (see Supplement 1, Fig. S5b). Thus, the response is broader than the spectrum of the laser pulse being sampled, leading to minor CEP effects on the sampled spectrum. Accordingly, the pump beam CEP was not calibrated.

We note that the enhanced field on the needle tip exhibits a phase shift of typically 0.2π to 0.5π compared to the incident field [40]. However, since both beams in nanoTiptoe experience the same shift due to the enhancement, the overall phase difference is zero and, therefore, does not affect the measurement. The excellent agreement between the nanoTiptoe measurement and the reference indicates a rather flat spectral response of the enhancement and demonstrates the capability of nanoTiptoe to sample near-petahertz laser fields. This conclusion is further supported by the similarity of the measured spectral phases obtained using both methods [see Fig. 2(b)]. The nanoTiptoe measurements are only slightly redshifted, as evident from the spectral amplitudes of the measured pulses in Fig. 2(b) and the calculated response (see Supplement 1, Fig. S5a). This difference relates to the response function of the nanometric needle tip. The good agreement of the time-domain waveforms indicates a secondary importance of this small redshift to most applications. Additionally, the agreement of the spectra with the spectrum recorded with a spectrometer suggests that the response in our experiments is broad enough to sample the full bandwidth without correction procedure, such as the typical Tiptoe reconstruction algorithms [22]. If there was an effect of side-peak ionization, the detected spectrum would be expected to be suppressed equally at both the low and high frequency edge (see Supplement 1). In our case, there is no such symmetric suppression but the small enhancement redshift, which actually boosts the low frequency part.

To further validate the nanoTiptoe technique for field sampling, we also performed scans of the dispersion of the signal pulse, its CEP, the field-strength ratio (see corresponding Supplement 1 sections), and its polarization. For the investigation of the polarization dependence, we kept the pump beam polarized along the tip axis and rotated the polarization of the signal beam [see Fig. 2(c)]. As the superposition of both beams drives the ionization process, we would expect a scaling of the signal in free-space as $\sim|\cos(\beta)|$, where β is the angle between the polarizations of the two laser pulses [solid blue line in Fig. 2(c)]. However, at a nanostructure, the pump beam generates surface normal near-fields that the signal beam can interfere with [cf. Fig. 1(c)] and [40]). Our polarization scan [Fig. 2(c)] suggests that the interference of the signal beam with surface normal near-fields has only a minor influence on the

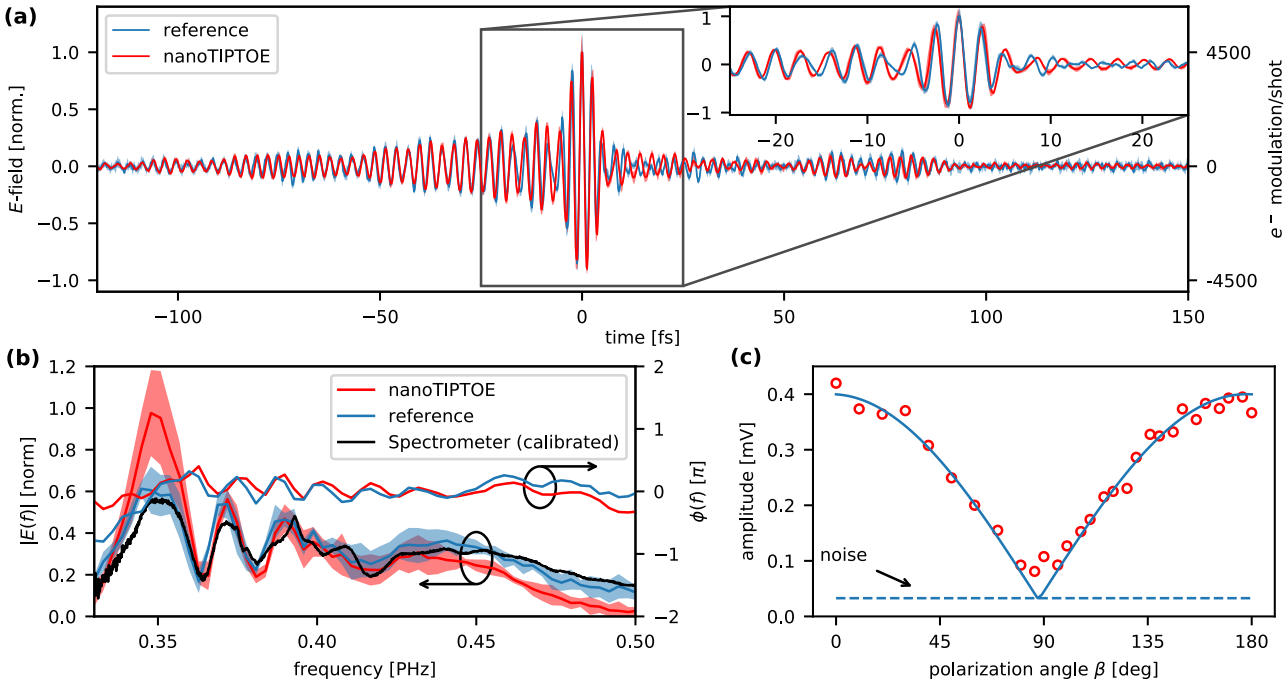

Fig. 2. Field measurement using nanoTIPTOE: (a) Average and standard deviation of five nanoTIPTOE field measurements in the center of the laser focus together with a reference obtained using TIPTOE in gas. The standard deviation is of the order of the linewidth. We corrected the data for a small offset by removing frequency components below 0.01 PHz. The enhanced intensities were $(7.2 \pm 0.9) \times 10^{13}\,\frac{\mathrm{W}}{\mathrm{cm}^2}$ and $(4.6 \pm 0.6) \times 10^{12}\,\frac{\mathrm{W}}{\mathrm{cm}^2}$ for the pump and signal beam in the nanoTIPTOE regime, respectively. The second axis indicates the current modulation in the nanoTIPTOE regime. The excellent agreement of nanoTIPTOE and standard TIPTOE can be seen in the inset. (b) Spectral amplitudes with error bar and spectral phase, obtained via a Fourier transform of the data in (a) as well as the calibrated spectrum recorded with a spectrometer. (c) Detected amplitudes depending on the polarization angle of the linearly polarized signal beam (red dots). As expected, the signal scales proportional to $|\cos(\beta)|$. The pump polarization remained the same.

signal taken with nanoTIPTOE, as the signal amplitude for perpendicular polarization nearly reaches the electronic noise amplitude [dashed blue line, Fig. 2(c)]. Therefore, nanoTIPTOE exhibits a polarization sensitivity that allows us to map the 2D polarization state.

The presented data demonstrate the applicability of nanoTIPTOE to a kilohertz repetition rate laser system. The application to higher repetition rate systems may be limited by damages of the tip, especially by heat accumulation [43] (see Supplement 1, Section 7). Additionally, the maximum incident intensity is limited by the tip damage threshold. In our experiments, however, we did not notice any significant damage of the tip, which can be confirmed by the repeatability of the measurements over time and is in agreement with related work (see Supplement 1, Section 7). Another limiting aspect is the nonlinearity of the ionization process ($\gtrapprox E^2$ in our case and up to E^8; see Supplement 1, Section 5). We see a fundamental limitation when the photon energy reaches the work function of the material, 4.5 eV [44] for tungsten. There, single photon absorption will lead to vanishing nonlinearity. The required minimum pulse energy of the signal beam to be sampled by nanoTIPTOE, given a sufficient pump intensity, is limited by the electronic noise level of the detection. We estimate that the lowest signal pulse energy that can be resolved is below 200 pJ at our conditions.

Having established that nanoTIPTOE provides the electric field waveform of the sampling field, we can now investigate how scanning the needle tip accross the focal plane provides spatially resolved data. Some care has to be taken in such scanning measurements. As the measured waveform samples only the relative phase between signal and pump pulse [23,24], the mode size of the pump beam has been made smaller by a factor of roughly 2.4, causing a larger focal spot size. This increase in size leads to a rather flat pump beam intensity and phase profile over the area that is scanned for the sampling pulse. In order to demonstrate the capability of nanoTIPTOE in spatiotemporal field sampling of near-petahertz fields, we sampled a light beam carrying OAM [28,29]. The signal beam was shaped by a vortex plate (Vortex Photonics V-780-20-1) that preserves linear polarization into an OAM beam. As the wave plate had a limited bandwidth, a suitable bandpass filter was added, which increased the pulse duration to 33 fs. The pump pulse, however, was not modified such that the temporal gate remained short. The vortex beam resulting from the beam shaping of the signal pulse is expected to exhibit a field distribution with a singularity on the propagation axis as well as a helical phase shape [cf. Figs. 1(a) and 3(c)].

In order to map the evolution of the vortex field in the focal plane, we scanned the tip through the beam while varying the delay over a few oscillations of the most intense part of the signal pulse. The result is depicted in Fig. 3(a). A clear rotational motion of the field amplitudes around the center of the focal spot is observable. The extracted amplitude and phase as a function of the needle tip position are shown in Figs. 3(b) and 3(d), together with a theoretical expectation for a Laguerre–Gaussian mode [(c) and e)]; see Supplement 1 for details. An animated version of Fig. 3(a) can be found in Visualization 1. The field distribution exhibits a typical doughnut shape, the minimum of which is visible in the middle despite the pump beam being maximal there. In order to validate that nanoTIPTOE provides full spectral resolution at every

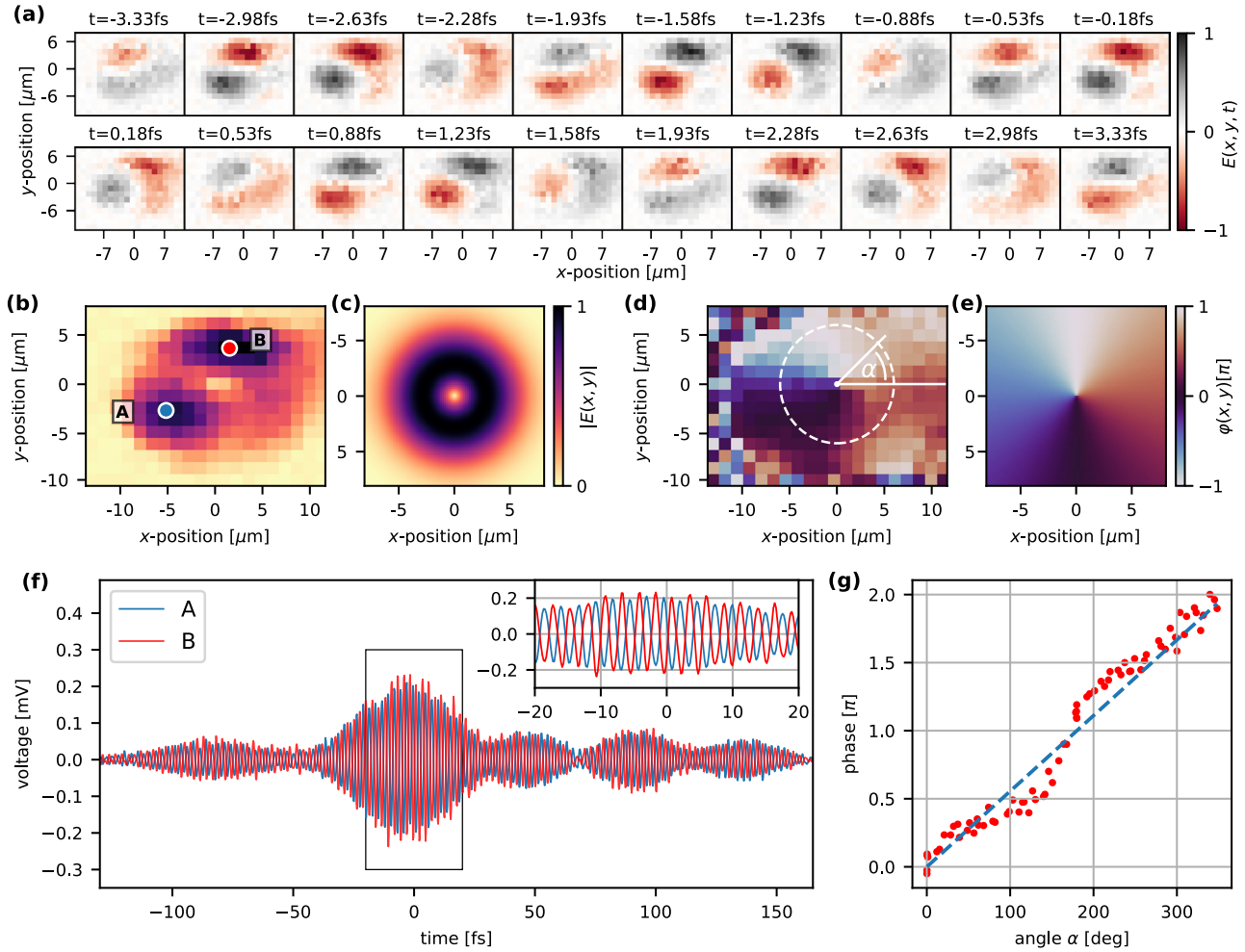

Fig. 3. Spatially resolved measurements of OAM beams: (a) Field amplitudes as a function of space and time, normalized to unity. (b) Amplitude of the measured current modulation induced by the OAM beam together with the expected shape for the theoretical Laguerre–Gaussian beam shown in (c). Deviations between experimental data and the simple OAM profile can be attributed to astigmatism in the focusing optics as well as to a non-Gaussian mode shape that has been used for the vortex generation. (d) The extracted phase at each point in the sampled plane exhibits a helical profile as theoretically shown in (e). The angle α defines a polar coordinate system. (f) Field sampling with nanoTIPTOE at the points A and B at opposite sides of the focus, indicated in (b). (g) The phase for each point within the dashed circle in (d) (red dots) shows a linear trend with α (dashed blue line). The raw data used for the plots in (a), (b), (d), and (g) can be seen in Figure S1 of Supplement 1. To generate the plot in (f), a Fourier filter from 0.1 to 1 PHz has been applied in order to remove nonlinear distortions.

point in space, we also performed scans over the full pulse length, but only at selected points marked as A and B in Fig. 3(b). The corresponding data was Fourier transform filtered and is shown in Fig. 3(f). The points A and B were chosen at opposite sides of the mode, since this is where we expect the spatial phase difference to be maximum. Indeed, the corresponding waveforms exhibit a clear π-phase difference, which is due to the OAM of the signal beam. As can be seen in Fig. 3(d), one of the main features of light carrying OAM, the helical phase front, agrees well with the theoretical prediction, Fig. 3(e). To quantify the spiral phase, we introduced a polar angle α and evaluated all phase points within the dashed circle in Fig. 3(d). We fixed the central point and calculated the corresponding α for every data point in the region of interest. The result [red dots in Fig. 3(g)] is in qualitative agreement with the expected linear increase of the phase with α. We attribute the small deviations from the linear scaling for $\alpha \in [120°: 220°]$ to a curved pulse front of the pump beam, which is even visible without vortex plate (see Supplement 1 for details).

4. CONCLUSION

In conclusion, we have demonstrated that nanoTIPTOE enables the spatially resolved measurement of near-petahertz optical field oscillations with sub-cycle resolution. The localized probe enabled the spatiotemporal characterization of optical fields by employing a nanometric needle tip instead of the conventional electrodes. The field enhancement allowed the characterization of laser fields with moderate intensity—a major advance compared to techniques requiring high-power laser sources. As compared to previous approaches for electronic field detection with nanotips, which were often limited to the low terahertz region [4,5], nanoTIPTOE increases the temporal resolution by nearly 3 orders of magnitude. While the detected bandwidth is comparable to that in [42] using attosecond streaking spectroscopy, the nanoTIPTOE approach is much simpler and avoids a complex vacuum beamline. A combination of nanoTIPTOE with latest approaches in time-resolved scanning tunneling microscopy [38,39] seems promising in characterizing the light-induced near-fields of a nanometric

sample with attosecond precision. Theoretically, the resolution here is limited by the interaction of the nanometric needle with the field close to the apex, as extensively studied in [40]. For our tip geometry, we expect a maximum resolution in the order of the tip diameter, and even down to 1 nm [45] using smaller tips. Finally, orienting the needle along the propagation direction of the laser beam [46] may pave the way toward the measurement of the longitudinal component of strongly focused light with nanoTIPTOE. Such measurements would offer a more detailed understanding of the properties of focused light in superresolution microscopy.

Funding. Deutsche Forschungsgemeinschaft (LMUexcellent, SPP1840); Max-Planck-Gesellschaft (Fellow program, IMPRS-APS, MPSP); Alexander von Humboldt-Stiftung; European Research Council (Advanced Grant AccelOnChip, FETlaunchpad FIELDTECH, FETopen PetaCOM); Office of Science (DE-AC02-76SF00515); Defense Threat Reduction Agency (HDTRA1-19-1-0026); Natural Sciences and Engineering Research Council of Canada; National Research Council Canada (Joint Centre for Extreme Photonics); University of Ottawa.

Acknowledgment. We are grateful for support by Ferenc Krausz providing suitable laboratories and for support by Thomas Nubbemeyer and Maximilian Seeger in laser operations. We acknowledge fruitful discussions with Matthew Weidman, Vladislav Yakovlev, Nicholas Karpowicz, and Ferenc Krausz. The experiments were carried out at LMU and MPQ. J. S. and A. M. acknowledge support by the Max Planck Society via the IMPRS for Advanced Photon Science. J. B. acknowledges support by the Max Planck School of Photonics. M. F. K. acknowledges support by the Max Planck Society via the Max Planck Fellow program. M. F. K.'s work at SLAC is supported by the U.S. Department of Energy, Office of Science, Basic Energy Sciences, Scientific User Facilities Division. P. B. C. acknowledges funds from the US Defense Threat Reduction Agency (DTRA) and the University of Ottawa. P. B. C. and A. S. acknowledge support from NRC Joint Centre for Extreme Photonics and also from the Natural Sciences and Engineering Research Council of Canada (NSERC).

Author contributions. J. B. and J. S. contributed equally to this work. J. S. and M. F. K. conceived the nanoTIPTOE concept. P. H. contributed expertise on nanometric needle tips. A. S., M. F. K., and P. C. conceived the experiment with OAM beams. J. B., J. S., A. M., and N. S. performed the measurements. Z. W. and P. R. supported laser operations. The data were analyzed by J. B. and J. S. The paper was written by J. B., J. S., B. B., and M. F. K. and reviewed by all authors.

Disclosures. The authors declare no competing interests.

Data availability. Data underlying the results presented in this paper are not publicly available at this time but may be obtained from the authors upon reasonable request.

Supplemental document. See Supplement 1 for supporting content.

REFERENCES

1. T. Brabec and F. Krausz, "Intense few-cycle laser fields: frontiers of nonlinear optics," Rev. Mod. Phys. **72**, 545–591 (2000).
2. F. Krausz and M. Ivanov, "Attosecond physics," Rev. Mod. Phys. **81**, 163–234 (2009).
3. T. L. Cocker, V. Jelic, R. Hillenbrand, and F. A. Hegmann, "Nanoscale terahertz scanning probe microscopy," Nat. Photonics **15**, 558–569 (2021).
4. D. Peller, C. Roelcke, L. Z. Kastner, T. Buchner, A. Neef, J. Hayes, F. Bonafé, D. Sidler, M. Ruggenthaler, A. Rubio, R. Huber, and J. Repp, "Quantitative sampling of atomic-scale electromagnetic waveforms," Nat. Photonics **15**, 143–147 (2021).
5. L. Wimmer, G. Herink, D. R. Solli, S. V. Yalunin, K. E. Echternkamp, and C. Ropers, "Terahertz control of nanotip photoemission," Nat. Phys. **10**, 432–436 (2014).
6. I. Pupeza, M. Huber, M. Trubetskov, *et al.*, "Field-resolved infrared spectroscopy of biological systems," Nature **577**, 52–59 (2020).
7. M. Neuhaus, J. Schötz, M. Aulich, A. Srivastava, D. Kimbaras, V. Smejkal, V. Pervak, M. Alharbi, A. M. Azzeer, F. Libisch, C. Lemell, J. Burgdörfer, Z. Wang, and M. F. Kling, "Transient field-resolved reflectometry at 50–100 THz," Optica **9**, 42–49 (2022).
8. M. Hentschel, R. Kienberger, C. Spielmann, G. A. Reider, N. Milosevic, T. Brabec, P. Corkum, U. Heinzmann, M. Drescher, and F. Krausz, "Attosecond metrology," Nature **414**, 509–513 (2001).
9. J. Itatani, F. Quéré, G. L. Yudin, M. Y. Ivanov, F. Krausz, and P. B. Corkum, "Attosecond streak camera," Phys. Rev. Lett. **88**, 173903 (2002).
10. R. Kienberger, E. Goulielmakis, M. Uiberacker, A. Baltuska, V. Yakovlev, F. Bammer, A. Scrinzi, T. Westerwalbesloh, U. Kleineberg, U. Heinzmann, M. Drescher, and F. Krausz, "Atomic transient recorder," Nature **427**, 817–821 (2004).
11. E. Goulielmakis, M. Uiberacker, R. Kienberger, A. Baltuska, V. Yakovlev, A. Scrinzi, T. Westerwalbesloh, U. Kleineberg, U. Heinzmann, M. Drescher, and F. Krausz, "Direct measurement of light waves," Science **305**, 1267–1269 (2004).
12. T. J. Hammond, G. G. Brown, K. T. Kim, D. M. Villeneuve, and P. B. Corkum, "Attosecond pulses measured from the attosecond lighthouse," Nat. Photonics **10**, 171–175 (2016).
13. A. S. Wyatt, T. Witting, A. Schiavi, D. Fabris, P. Matia-Hernando, I. A. Walmsley, J. P. Marangos, and J. W. G. Tisch, "Attosecond sampling of arbitrary optical waveforms," Optica **3**, 303–310 (2016).
14. Y. H. Kim, I. A. Ivanov, S. I. Hwang, K. Kim, C. H. Nam, and K. T. Kim, "Attosecond streaking using a rescattered electron in an intense laser field," Sci. Rep. **10**, 22075 (2020).
15. S. Keiber, S. Sederberg, A. Schwarz, M. Trubetskov, V. Pervak, F. Krausz, and N. Karpowicz, "Electro-optic sampling of near-infrared waveforms," Nat. Photonics **10**, 159–162 (2016).
16. A. Korobenko, K. Johnston, M. Kubullek, L. Arissian, Z. Dube, T. Wang, M. Kübel, A. Y. Naumov, D. M. Villeneuve, M. F. Kling, P. B. Corkum, A. Staudte, and B. Bergues, "Femtosecond streaking in ambient air," Optica **7**, 1372–1376 (2020).
17. D. Zimin, M. Weidman, J. Schötz, M. F. Kling, V. S. Yakovlev, F. Krausz, and N. Karpowicz, "Petahertz-scale nonlinear photoconductive sampling in air," Optica **8**, 586–590 (2021).
18. S. B. Park, K. Kim, W. Cho, S. I. Hwang, I. Ivanov, C. H. Nam, and K. T. Kim, "Direct sampling of a light wave in air," Optica **5**, 402–408 (2018).
19. N. Saito, N. Ishii, T. Kanai, and J. Itatani, "All-optical characterization of the two-dimensional waveform and the Gouy phase of an infrared pulse based on plasma fluorescence of gas," Opt. Express **26**, 24591–24601 (2018).
20. S. I. Hwang, S. B. Park, J. Mun, W. Cho, C. H. Nam, and K. T. Kim, "Generation of a single-cycle pulse using a two-stage compressor and its temporal characterization using a tunnelling ionization method," Sci. Rep. **9**, 1613 (2019).
21. W. Cho, S. I. Hwang, C. H. Nam, M. R. Bionta, P. Lassonde, B. E. Schmidt, H. Ibrahim, F. Légaré, and K. T. Kim, "Temporal characterization of femtosecond laser pulses using tunneling ionization in the UV, visible, and mid-IR ranges," Sci. Rep. **9**, 16067 (2019).
22. W. Cho, J.-U. Shin, and K. T. Kim, "Reconstruction algorithm for tunneling ionization with a perturbation for the time-domain observation of an electric-field," Sci. Rep. **11**, 13014 (2021).
23. M. R. Bionta, F. Ritzkowsky, M. Turchetti, Y. Yang, D. Cattozzo Mor, W. P. Putnam, F. X. Kärtner, K. K. Berggren, and P. D. Keathley, "On-chip sampling of optical fields with attosecond resolution," Nat. Photonics **15**, 456–460 (2021).
24. Y. Liu, S. Gholam-Mirzaei, J. E. Beetar, J. Nesper, A. Yousif, M. Nrisimhamurty, and M. Chini, "All-optical sampling of few-cycle infrared pulses using tunneling in a solid," Photon. Res. **9**, 929–936 (2021).
25. Y. Liu, J. E. Beetar, J. Nesper, S. Gholam-Mirzaei, and M. Chini, "Single-shot measurement of few-cycle optical waveforms on a chip," Nat. Photonics **16**, 109–112 (2022).
26. J. Zhao, Y. E. K. Williams, X.-C. Zhang, and R. W. Boyd, "Spatial sampling of terahertz fields with sub-wavelength accuracy via probe-beam encoding," Light Sci. Appl. **8**, 55 (2019).
27. O. Mitrofanov, L. Viti, E. Dardanis, M. C. Giordano, D. Ercolani, A. Politano, L. Sorba, and M. S. Vitiello, "Near-field terahertz probes with room-temperature nanodetectors for subwavelength resolution imaging," Sci. Rep. **7**, 44240 (2017).
28. L. Allen, M. W. Beijersbergen, R. J. C. Spreeuw, and J. P. Woerdman, "Orbital angular momentum of light and the transformation of Laguerre-Gaussian laser modes," Phys. Rev. A **45**, 8185–8189 (1992).
29. A. M. Yao and M. J. Padgett, "Orbital angular momentum: origins, behavior and applications," Adv. Opt. Photon. **3**, 161–204 (2011).
30. L. Rego, K. M. Dorney, N. J. Brooks, Q. L. Nguyen, C.-T. Liao, J. S. Román, D. E. Couch, A. Liu, E. Pisanty, M. Lewenstein, L. Plaja, H. C. Kapteyn, M. M. Murnane, and C. Hernández-García, "Generation

of extreme-ultraviolet beams with time-varying orbital angular momentum," Science **364**, eaaw9486 (2019).
31. Y. Fang, Z. Guo, P. Ge, Y. Dou, Y. Deng, Q. Gong, and Y. Liu, "Probing the orbital angular momentum of intense vortex pulses with strong-field ionization," Light Sci. Appl. **11**, 34 (2022).
32. J. Wätzel and J. Berakdar, "Electrons in intense laser fields with local phase, polarization, and skyrmionic textures," Phys. Rev. A **102**, 063105 (2020).
33. J. Wätzel and J. Berakdar, "Spatiotemporal delay in photoionization by polarization-structured laser fields," Phys. Rev. A **103**, 063107 (2021).
34. Y. Dai, Z. Zhou, A. Ghosh, S. Yang, C.-B. Huang, and H. Petek, "Ultrafast nanofemto photoemission electron microscopy of vectorial plasmonic fields," MRS Bull. **46**, 738–746 (2021).
35. Y. Dai, Z. Zhou, A. Ghosh, K. Kapoor, M. Dąbrowski, A. Kubo, C.-B. Huang, and H. Petek, "Ultrafast microscopy of a twisted plasmonic spin skyrmion," Appl. Phys. Rev. **9**, 011420 (2022).
36. B. Barwick, C. Corder, J. Strohaber, N. Chandler-Smith, C. Uiterwaal, and H. Batelaan, "Laser-induced ultrafast electron emission from a field emission tip," New J. Phys. **9**, 142 (2007).
37. D. Hoff, M. Krüger, L. Maisenbacher, A. M. Sayler, G. G. Paulus, and P. Hommelhoff, "Tracing the phase of focused broadband laser pulses," Nat. Phys. **13**, 947–951 (2017).
38. M. Garg and K. Kern, "Attosecond coherent manipulation of electrons in tunneling microscopy," Science **367**, 411–415 (2020).
39. M. Garg, A. Martin-Jimenez, M. Pisarra, Y. Luo, F. Martín, and K. Kern, "Real-space subfemtosecond imaging of quantum electronic coherences in molecules," Nat. Photonics **16**, 196–202 (2022).
40. S. Thomas, G. Wachter, C. Lemell, J. Burgdörfer, and P. Hommelhoff, "Large optical field enhancement for nanotips with large opening angles," New J. Phys. **17**, 063010 (2015).
41. S. V. Yalunin, M. Gulde, and C. Ropers, "Strong-field photoemission from surfaces: theoretical approaches," Phys. Rev. B **84**, 195426 (2011).
42. J. Schötz, B. Förg, M. Förster, W. A. Okell, M. I. Stockman, F. Krausz, P. Hommelhoff, and M. F. Kling, "Reconstruction of nanoscale near fields by attosecond streaking," IEEE J. Sel. Top. Quantum Electron. **23**, 77–87 (2017).
43. N. Pfullmann, C. Waltermann, M. Noack, S. Rausch, T. Nagy, C. Reinhardt, M. Kovačev, V. Knittel, R. Bratschitsch, D. Akemeier, A. Hütten, A. Leitenstorfer, and U. Morgner, "Bow-tie nano-antenna assisted generation of extreme ultraviolet radiation," New J. Phys. **15**, 093027 (2013).
44. H. B. Michaelson, "The work function of the elements and its periodicity," J. Appl. Phys. **48**, 4729–4733 (1977).
45. S. Thomas, M. Krüger, M. Förster, M. Schenk, and P. Hommelhoff, "Probing of optical near-fields by electron rescattering on the 1 nm scale," Nano Lett. **13**, 4790–4794 (2013).
46. A. Bouhelier, M. Beversluis, A. Hartschuh, and L. Novotny, "Near-field second-harmonic generation induced by local field enhancement," Phys. Rev. Lett. **90**, 013903 (2003).